

## Relationships between Precipitation Anomalies in Uruguay and Southern Brazil and Sea Surface Temperature in the Pacific and Atlantic Oceans

ALVARO F. DIAZ

*Instituto de Mecánica de los Fluidos e Ingeniería Ambiental, Universidad de la República, Montevideo, Uruguay*

CAAREM D. STUDZINSKI

*Centro de Previsão do Tempo e Estudos Climáticos, Instituto Nacional de Pesquisas Espaciais, Cachoeira Paulista, Sao Paulo, Brazil*

CARLOS R. MECHOSO

*Department of Atmospheric Sciences, University of California, Los Angeles, Los Angeles, California*

(Manuscript received 10 September 1996, in final form 23 April 1997)

### ABSTRACT

This study focuses on precipitation in Uruguay and the Brazilian state of Rio Grande do Sul, which extend along the Atlantic coast of southern South America. The present paper has two principal goals: 1) to describe the annual cycle of precipitation and 2) to investigate the relationships between its anomalies and those in sea surface temperature (SST) in the Pacific and Atlantic oceans. The dataset is provided by 40 rainfall stations almost evenly distributed in space and covers the period 1917–80. The tools used in support of this research include principal component and canonical correlation analyses.

It is found that total precipitation tends to be evenly distributed during the year. The largest spatial variability in the monthly deviations from the annual mean appears as a west–east (inland–coastal) dipole with the largest positive values in the west during early fall and midspring, and in the east along the Atlantic coast during winter. The second mode of rainfall variability appears as a north–south dipole with the largest positive values in the south during late summer and late fall, and in the north during early spring and early summer. The third mode appears primarily as a north–south dipole along the western boundary with the largest positive values in the southwest during fall and in the northwest during early spring. These modes explain 60%, 19%, and 8% of the total variance. Five subregions are identified according to similarities between the characteristics of the annual cycles in their rainfall stations.

It is shown that there are significant relationships between anomalies in rainfall and in SST in the Pacific and Atlantic oceans. Some of these relationships confirm the results of previous studies, such as the links between the El Niño–Southern Oscillation phenomenon in the equatorial Pacific Ocean and rainfall anomalies in Uruguay during late spring–early summer and late fall–early winter. Other relationships have not been reported before, such as the links between SST anomalies in the southwestern Atlantic Ocean and rainfall anomalies in the entire region during October–December and April–July. It is also found that when SST anomalies are considered in both oceans simultaneously, their links with rainfall anomalies are in some cases enhanced and in others weakened.

### 1. Introduction

For Uruguay and the Brazilian state of Rio Grande do Sul (URSOL), whose economies are based on agricultural products and the use of hydroelectric power, a better understanding of the climatology, variability, and potential predictability of local precipitation is of primary importance. Our study focuses on that region,

which extends along the Atlantic coast of South America roughly east of 58.5°W, between 27° and 35°S. We have two principal goals in reference to the local precipitation: 1) to describe its annual cycle, and 2) to investigate the relationship between its anomalies and those in sea surface temperature (SST) in the Pacific and Atlantic oceans. The tools used for investigation include principal component and canonical correlation analyses.

Previous studies on precipitation for regions that include either all or part of URSOL strongly support the existence of links between precipitation anomalies and SST anomalies in the Pacific Ocean. For a region that includes URSOL, Ropelewski and Halpert (1987, 1989) demonstrated that rainfall during the period November–

---

*Corresponding author address:* Ing. Alvaro F. Díaz, Facultad de Ingeniería, Instituto de Mecánica de los Fluidos e Ingeniería Ambiental, Julio Herrera y Reissig 565, Montevideo 11300, Uruguay.  
E-mail: adiaz@fing.edu.uy

February tends to be above the median in El Niño years, whereas that during the period June–December tends to be below the median in years with a high value of the Southern Oscillation (SO) index (cold events in the equatorial Pacific Ocean). For southern South America, Lau and Sheu (1988) showed that years with warm SST events in the equatorial Pacific are associated with precipitation that is above the median. For Brazil, Rao and Hada (1990) found a significant negative correlation between precipitation during the austral autumn and spring seasons and the SO index. For Uruguay, Pisciotano et al. (1994) used long records of data provided by a dense network of rainfall stations to investigate precipitation anomalies during the extreme phases of El Niño–Southern Oscillation (ENSO). They demonstrated that rainfall during the period November–January tends to be above the median in El Niño years, as well as from March through July of the following years. They also found that rainfall during the period October–December tends to be below the median in years with a high SO index, as well as from March through July of the following years. Aceituno (1988) reported that the SO index and rainfall in the Paraná River basin are negatively correlated in the period November–December.

These results on rainfall have been indirectly supported by analyses of the streamflow variability in major rivers of the region. For example, Mechoso and Pérez (1992) showed that there is a clear tendency for the streamflow in the Negro and the Uruguay Rivers to be below the median during the period June–December in years with a high SO index and a slight tendency to be above the median during the period November–February in El Niño years, with values that are occasionally well above the median.

The influence of SST anomalies in the Atlantic Ocean on precipitation anomalies in URSOL has not yet been comprehensively examined to our knowledge. In principle, such an influence can be expected since the eastern coast of southern South America is an area of cyclogenesis, which can be sensitive to lower boundary conditions. Our study explores that issue, as well as the combined effects of concurrent SST anomalies in the Pacific and Atlantic oceans.

We start in section 2 by listing the datasets used in this study. In section 3, we analyze the annual mean precipitation and its spatial variability in the region selected for investigation. In section 4, we describe the methodology used in support of our search for relationships between anomalies in rainfall and SST. Sections 5, 6, and 7 present the results obtained for the periods selected, namely, November–February, October–December, and April–July, respectively. The cases of SST anomalies in the Pacific, Atlantic, and Pacific and Atlantic oceans are described separately in these sections. Section 8 discusses two case studies, one of which is of highly anomalous rainfall. Section 9 summarizes our results and presents our conclusions.

## 2. Datasets

The data for rainfall used in this study are monthly totals for 33 stations reporting continuously during the period January 1917–December 1980 and 7 stations reporting continuously between 1946 and 1980. The stations are almost evenly distributed in the region. The corresponding dataset was compiled by the Dirección Nacional de Meteorología (DINAMET, Uruguay), Instituto de Pesquisas Agronómicas do Rio Grande do Sul (IPAGRO, Brazil), and Instituto Nacional de Meteorologia (INEMET, Brazil). To study the spatial variability of the annual cycle in climatological rainfall (see section 3), we use the data from the 33 stations that report during the period January 1917–December 1980. To study the relationships between precipitation anomalies in URSOL and SST anomalies in the Pacific and Atlantic oceans (see section 4), we consider the reports from all 40 stations that report in the period 1946–80, which is thus taken as the analysis period. The SST fields are based on monthly means from the Global Ocean–Global Atmosphere (GOGA) dataset (Lau and Nath 1990) and cover the latitude band 42.5°S–25°N of the Pacific and Atlantic oceans with a resolution of 7.5° long  $\times$  4.5° lat. (This gives 132 grid points for the Atlantic and 314 for the Pacific.) The quality of the GOGA SST dataset is higher after 1946 than before that date. To account for the variations of grid size with latitude, the SST data were multiplied by the square root of the cosine of the latitude of the corresponding grid point.

## 3. Annual mean and variability in rainfall in URSOL

Figure 1 shows that annual mean rainfall in URSOL is largest in the northern sector, where values strongly decrease toward the Atlantic Ocean. The distribution is more uniform in the southern sector, with minima in the southwest and southeast of the region. The annual cycle has considerable spatial variability. For example, works by Prohaska (1976) and Pisciotano et al. (1994) show that rainfall in the western sector has an absolute maximum in March–April and a second peak in October. Further, southern and eastern Uruguay have a less pronounced seasonal cycle with a weak maximum during the austral winter.

To examine in detail the spatial variability of the annual cycle in climatological rainfall, we express the monthly mean values corresponding to each of the stations as percentages of their annual mean. Hereafter, the values resulting from this operation will be referred to as climatological monthly rainfalls in percentage, or CMRPs. The use of CMRPs emphasizes differences in phase, rather than in magnitude, between rainfall in different stations. Next, we proceed in two steps following an approach similar to that in the paper by Logue (1984).

As a first step, we obtain the annual cycle of the CMRPs averaged over all stations. The results of this

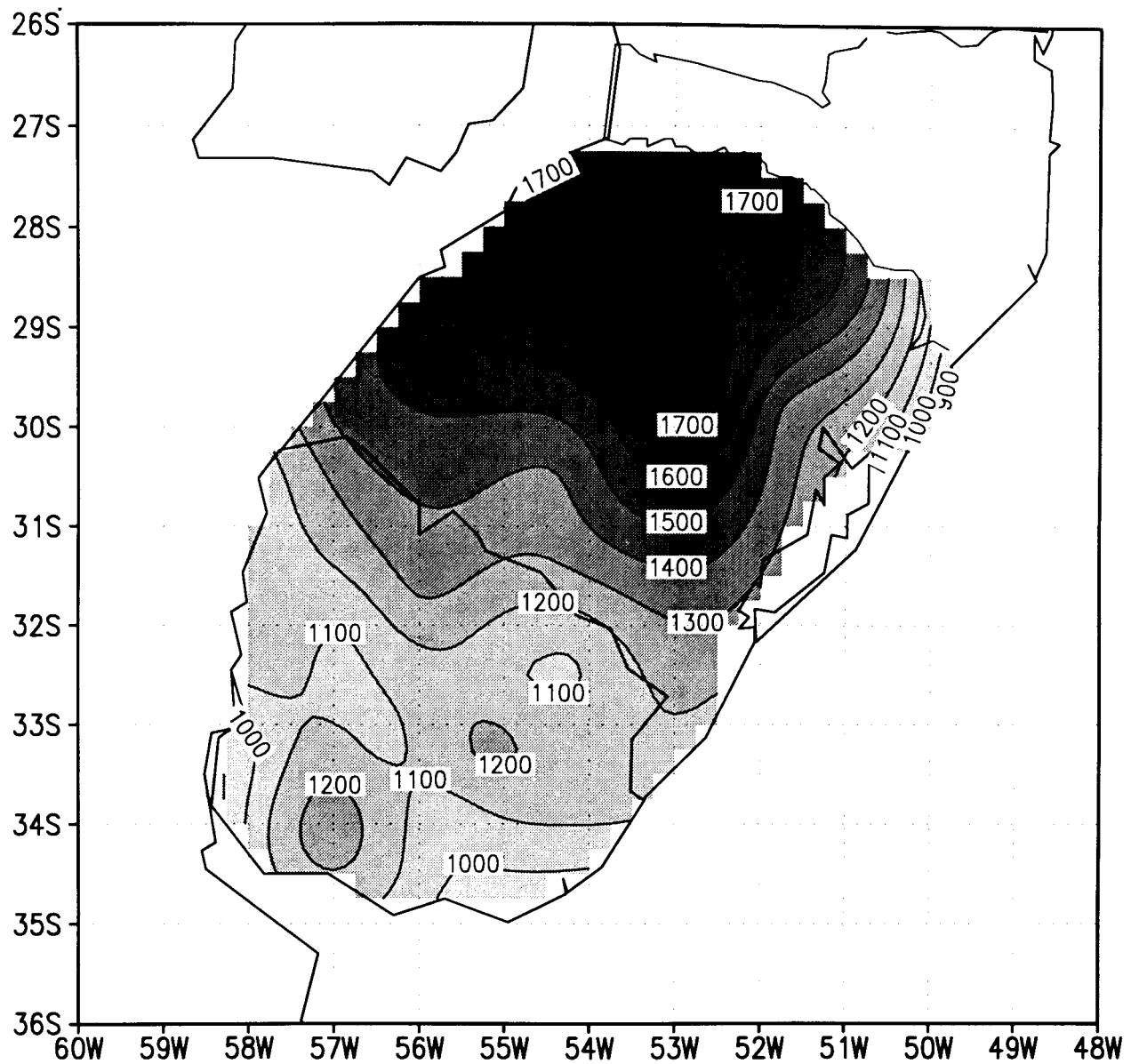


FIG. 1. Annual mean rainfall (mm) in URSOL for the period 1917-80.

exercise (see Fig. 2) give the monthly contribution to the annual mean rainfall over URSOL. Figure 2 shows that this contribution tends to be evenly distributed throughout the year, which implies that there are neither rainy nor dry seasons in the region. Nevertheless, there is a slight tendency for September–October and March–April to be the rainiest periods in the annual cycle and for November–December to be the driest period.

In the second step, we apply the method of principal component (PC) analysis to the 12 monthly CMRPs for each of the stations. First, we form the matrix (**F**) of the deviations of CMRPs with respect to the all-station mean for the corresponding month (shown in Fig. 2). The matrix **F** is organized into 12 rows (months) and

33 columns (stations). Second, we determine the covariance matrix ( $\mathbf{FF}^T/32$ ). We use the covariance matrix instead of the correlation matrix since the variables considered are expressed in the same units. Last, we determine the eigenvalues [ $\lambda(12)$ ] and eigenvectors [ $\mathbf{E}(12 \times 12)$ ] of the covariance matrix. The PCs are the rows of the matrix **C** ( $12 \times 33$ ), defined by the following relationship:

$$\mathbf{F} = \mathbf{E} \times \mathbf{C}. \quad (1)$$

The first three PCs found in this way account for 60%, 19%, and 9%, respectively, of explained variance. Each of these modes is statistically separable from sampling errors according to the test of North et al. (1982). The

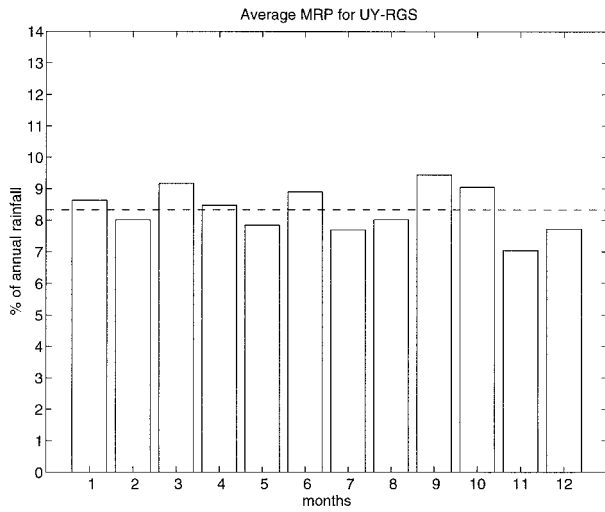


FIG. 2. Climatological monthly rainfalls in percent (CMRPs) for 1917–80 averaged over all stations in URSOL (Jan–Dec). The dotted line represents the mean value.

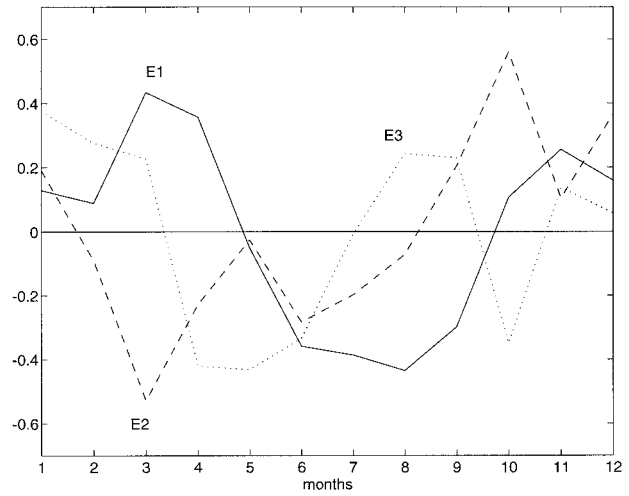


FIG. 4. First three eigenvectors of CMRP (Jan–Dec): E1 (solid), E2 (dashed), and E3 (dotted).

remaining modes account for very small fractions of the variance and have been considered statistically and presumably physically nonsignificant. We will display these PCs as contour plots in which each station is assigned the value of the element in C at the intersection of the row corresponding to the PC with the column corresponding to the station. The amount of the total variance explained by each PC is given by the eigenvalues of the covariance matrix.

PC1 (see Fig. 3a) is characterized by west–east contrasts. The corresponding eigenvector (see Fig. 4) has a strong annual component with positive values from early spring to midfall, which peak in early fall and midspring. The negative values have the largest magnitudes in winter. The largest variability, therefore, appears as a west–east (inland–coastal) dipole with the largest positive departures from the annual mean in the

west during early fall and midspring, and in the east along the Atlantic coast during winter. PC2 (see Fig. 3b) shows predominantly south–north contrasts. The corresponding eigenvector (see Fig. 4) has minima in late summer and late fall, and maxima in early spring and early summer. The second mode of rainfall variability, therefore, appears as a south–north dipole with the largest positive departures from the annual mean in the south during late summer and late fall, and in the north during early spring and early summer. PC3 (see Fig. 3c) shows a south–north dipole along the western boundary of the region. The corresponding eigenvector (see Fig. 4) has a maximum in summer, a stronger minimum in fall, and a weaker minimum in early spring. The third mode of variability, therefore, appears primarily as a north–south dipole along the western boundary of the region, with the largest positive departures from the annual mean in southwestern Uruguay during

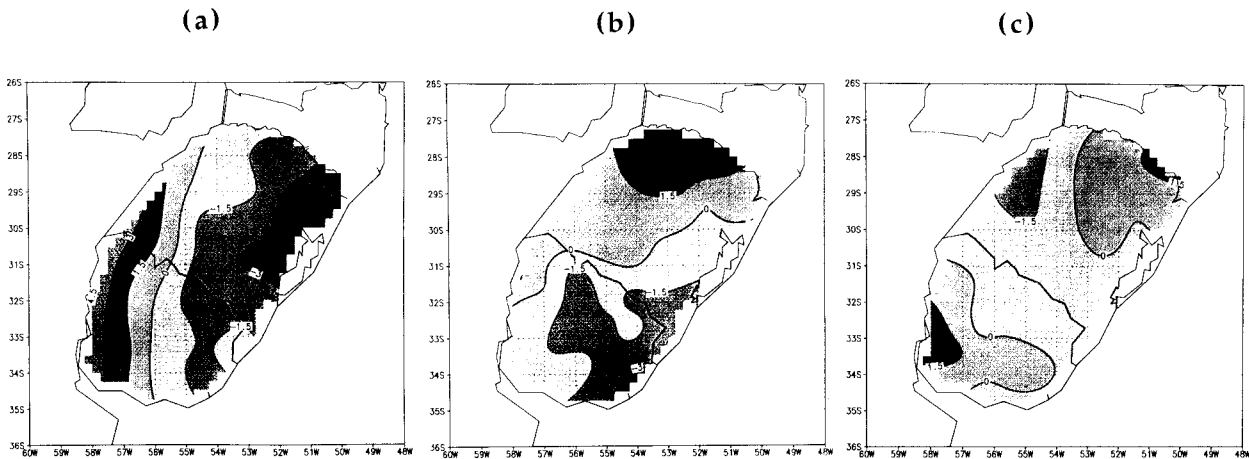


FIG. 3. First three principle components of CMRP: (a) PC1, (b) PC2, and (c) PC3.

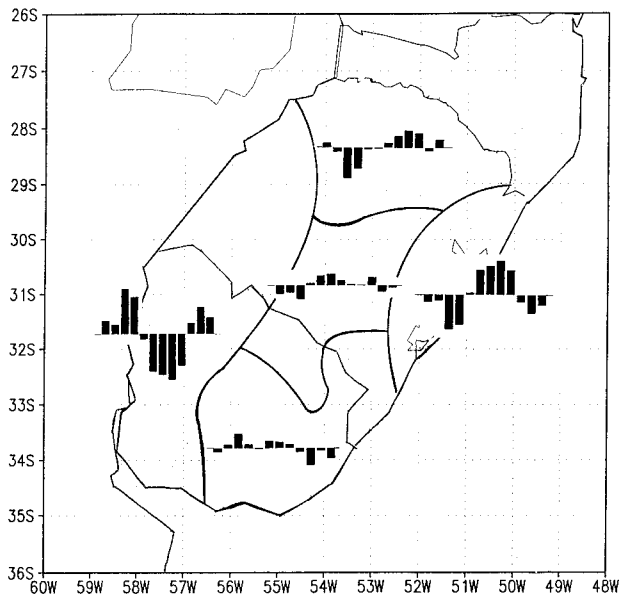


FIG. 5. As in Fig. 2 except for deviations from the annual mean in that each panel shows values representative of the particular figure subregion.

fall and in northwestern Rio Grande do Sul during early spring.

The higher variability in the western (inland) sector during midspring and early fall can develop as convective activity is enhanced by the interaction of frontal systems migrating from high latitudes with moist air from the Tropics. This enhanced convective activity in the western sector is associated with subsidence and the establishment of the “dry” season in the eastern sector. The higher variability in the eastern (coastal) sector during winter can develop in association with cyclogenesis over South America, which is most active at this time of the year (Gan and Rao 1991). In this case, the western and northern sectors would be in an area of subsidence consistent with a dry period. The results obtained for the northern sector are consistent with the behavior described by Rao and Hada (1990), who analyzed the characteristics of rainfall over Brazil using monthly rainfall data for a 21-yr period. These authors found that the rainiest season in southern Brazil is spring for the central part, summer for the western part, and winter for the eastern (coastal) part. During spring, southern Brazil (i.e., the northern sector of URSOL) is reached by mesoscale convective complexes that develop over Paraguay and move eastward along the equatorward side of the subtropical jet stream (Velasco and Fritsch 1987; Silva Dias 1987).

We next consider the matrix ( $\mathbf{F}_3$ ) defined as in (1), except that we only take the first three columns of  $\mathbf{E}$  and the first three rows of  $\mathbf{C}$ . The matrix  $\mathbf{F}_3$  defined in this way gives the components of  $\mathbf{F}$  that are associated with the principal modes of rainfall variability. An inspection of the columns of  $\mathbf{F}_3$  allows us to subjectively

TABLE 1. Periods of strongest deviations of CRMPs with respect to the all-station mean.

Sector of URSOL	Strongest positive	Strongest negative
Western	March–April	June–September
Southern	June–August	October–December
Eastern and central	June–September	March–April (October–December)
Northern	March–May	September–October

divide URSOL into five sectors according to the similarities between the characteristics of the annual cycle of deviations of CRMPs with respect to the all-station mean (see Fig. 5).

The periods of strongest positive and negative deviations from the annual cycle are shown in Table 1. The eastern and central sectors primarily differ in the amplitude of their annual cycle in CRMPs. There is a clear opposition in phase between the western (inland) and the eastern (coastal) sectors, which have the largest annual cycles. There are strong negative values in the period October–December in both coastal sectors. On the other hand, the southern sector is the only one that shows values with weak magnitudes during the first part of the year. These results for Uruguay are consistent with those obtained by using a method based on cluster analysis by Terra and Pisciotto (1994).

#### 4. Relationships between anomalies in rainfall and SST: Methodology

We use the method of canonical correlation analysis (CCA), which is a linear multivariate technique. The reader is referred to Barnett and Preisendorfer (1987, hereafter BP87), Preisendorfer (1988), and Graham et al. (1987a,b) for a detailed description of the CCA method. In our version of the method, the input consists of the empirical orthogonal functions (EOFs) and their corresponding PCs of SST and rainfall anomalies. We retain the EOFs that explain at least 80% of the variance of the corresponding field. Let  $p$  and  $q$  be the number of EOFs retained for the SST anomalies and rainfall anomalies, respectively (our 80% requirement on the EOFs resulted in  $p > q$  for all cases). The time series of the PCs retained is standardized so that their norm is 1.

The method produces  $p$  and  $q$  linear combinations of the standardized time series of the PCs for the SST and rainfall anomalies, respectively. These linear combinations— $u_i(t)$  and  $v_i(t)$ , where  $t$  is time—and their correlations,  $\mu_i$ , are called canonical component vectors and canonical correlation coefficients when they satisfy the following requirements: 1)  $|\mu_1|$  is maximum and 2)  $u_i$  and  $v_i$  are uncorrelated with  $u_j$  and  $v_j$  if  $i \neq j$ . The absolute values of  $\mu_i$  are organized to decrease with increasing  $i$ . In the CCA, canonical modes do not necessarily explain decreasing amounts of variance. The SST and rainfall anomaly fields can be represented in

TABLE 2. Cumulative sum of fractional rainfall variance explained by the first  $q$  SST canonical vectors for each case considered in this study.

	$q = 1$	$q = 1, 2$	$q = 1, \dots, 3$	$q = 1, \dots, 4$	$q = 1, \dots, 5$	$q = 1, \dots, 6$	$q = 1, \dots, 7$
November–February							
Pacific	0.29	0.32	0.36	0.41	0.42	0.43	0.44
Atlantic	0.33	0.41	0.43	0.44	0.47	0.48	0.48
Pacific–Atlantic	0.27	0.33	0.49	0.50	0.51	0.52	0.53
October–December							
Pacific	0.17	0.39	0.43	0.46	0.47	0.48	
Atlantic	0.37	0.45	0.48	0.50	0.51	0.52	
Pacific–Atlantic	0.28	0.44	0.49	0.51	0.54	0.55	
April–July							
Pacific	0.10	0.19	0.24	0.26	0.35		
Atlantic	0.33	0.35	0.39	0.42	0.42		
Pacific–Atlantic	0.12	0.29	0.36	0.45	0.47		

terms of the canonical component vectors and the canonical maps— $g_i(\lambda, \phi)$  and  $h_i(\lambda, \phi)$ , where  $\lambda$  is longitude and  $\phi$  is latitude—in the following way:

$$\sum_1^p u_j(t) g_j(\lambda, \phi) \quad \text{and} \quad \sum_1^q v_j(t) h_j(\lambda, \phi), \quad (2)$$

respectively. The canonical maps show the correlations at specific locations between the canonical vectors  $u_i$ ,  $v_i$ , and the time series of the SST and rainfall anomalies fields reconstructed from the first  $p$  and  $q$  EOFs, respectively. To estimate the significance of the values in the canonical maps, we use a standard Student's  $t$ -test. The significant values form the most relevant patterns of simultaneous variability for both fields.

Our selection of periods to be investigated is based on the findings of previous studies that have targeted rainfall variability in regions covering (partially or totally) URSOL. The following considerations support our selection of the periods November–February, October–December, and April–July.

- Ropelewski and Halpert (1987) showed that rainfall during the period November–February tends to be above the median in El Niño years in a region that includes URSOL.
- The same authors (Ropelewski and Halpert 1989) showed that rainfall during the period June–December tends to be below the median in years with a high value of the SO index. Pisciottano et al. (1994) found that rainfall over Uruguay during the period October–December tends to be below the median for years with high SO index.
- For Uruguay, Pisciottano et al. (1994) demonstrated that rainfall during the period March–July for years following El Niño years tends to be above the median and that rainfall during the same period after years with high values of the SO index tends to be below the median. More recent analyses of these relationships for URSOL (G. Pisciottano 1995, personal communication) have shown that these relationships are

stronger in the period April–July, especially in northern Uruguay and Rio Grande do Sul.

Note that the criteria for selection of the periods for analysis did not include specific considerations on the influence of Atlantic SST anomalies on precipitation in URSOL. Previous studies do not provide much guidance in this regard. The selection of three periods (November–February, October–December, and April–July) and of three configurations of SST anomalies (Pacific, Atlantic, and Pacific–Atlantic) gives a total of nine cases to be analyzed. The results obtained in the analyses are discussed separately in the following three sections of this paper. In most cases, we will focus on the first canonical mode ( $p = q = 1$ ), which explains most of the variance (see Table 2).

## 5. Relationships between anomalies in rainfall and SST: November–February

### a. SST anomalies in the Pacific Ocean

In this case (see Fig. 6), the correlation between  $u_1$  and  $v_1$  is 0.86, which implies that the patterns of SST and rainfall anomalies associated with the first canonical modes tend to have the *same* correspondence in sign as  $g_1$  and  $h_1$ . Figure 6 shows that  $g_1$  has mostly positive values north of about 10°S and mostly negative values south of that latitude. There are significant positive values of  $g_1$  in the central and eastern equatorial Pacific (CEEP) and in the central South Pacific, and significant negative values in the southwestern tropical Pacific (SWTP). Figure 6 also shows that  $h_1$  has positive and mostly significant values. The only sectors with non-significant values of  $h_1$  are along the northeastern boundary of URSOL, and central and southeastern Uruguay. These results support the existence of relationships between wet (dry) rainfall anomalies in the central sector of URSOL and warm (cold) SST anomalies in the ENSO region of the Pacific Ocean simultaneous with cold

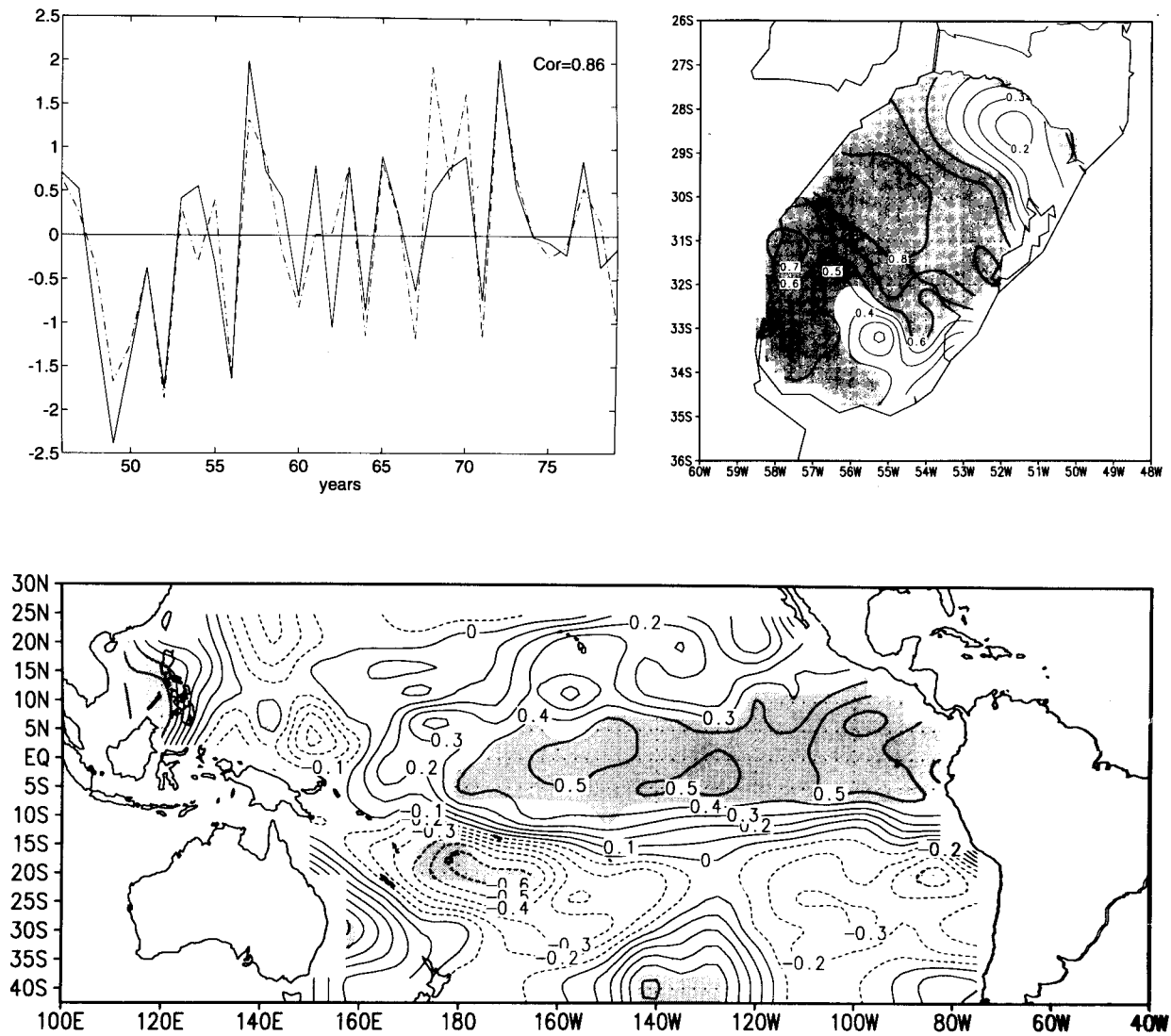


FIG. 6. First canonical vectors and canonical patterns for Nov–Feb and SST anomalies in the Pacific Ocean: (upper left)  $u_1$  (solid) and  $v_1$  (dashed), (upper right)  $h_1$ , and (bottom)  $g_1$ . Shaded areas represent sectors with values that are significant at the 95% level.

(warm) SST anomalies in the South Pacific convergence zone (SPCZ) region.

*b. SST anomalies in the Atlantic Ocean*

In this case (see Fig. 7), the correlation between  $u_1$  and  $v_1$  is  $-0.91$ , which implies that the patterns of SST and rainfall anomalies associated with the first canonical modes tend to have the *opposite* correspondence in sign as  $g_1$  and  $h_1$ . Figure 7 shows that  $g_1$  has positive values everywhere except in the South Atlantic. We can identify four sectors with significant values: 1) the southwestern subtropical Atlantic (SWSA) eastward of URSOL, 2) the eastern equatorial Atlantic (EEQA), 3) the western equatorial Atlantic (WEQA), and 4) the northwestern tropical Atlantic (NWTa). Figure 7 also shows that  $h_1$  has negative and mostly significant values in

URSOL, except for the southern sector. These results support the existence of relationships between wet (dry) rainfall anomalies in the northern sector of URSOL and warm (cold) SST anomalies in both the South Atlantic convergence zone (SACZ) region and the equatorial Atlantic Ocean except for a narrow band in the central part around  $15^\circ\text{W}$ .

*c. SST anomalies in the Pacific and Atlantic oceans*

In this case (see Fig. 8), the correlation between  $u_1$  and  $v_1$  is  $-0.92$ , whose absolute value is only slightly larger than those obtained by considering individual ocean basins. Figure 8 shows that the patterns of  $g_1$  in the Pacific and Atlantic are quite similar to those obtained by using the SST anomalies in each ocean basin (see Figs. 6 and 7, respectively). Nevertheless, there are

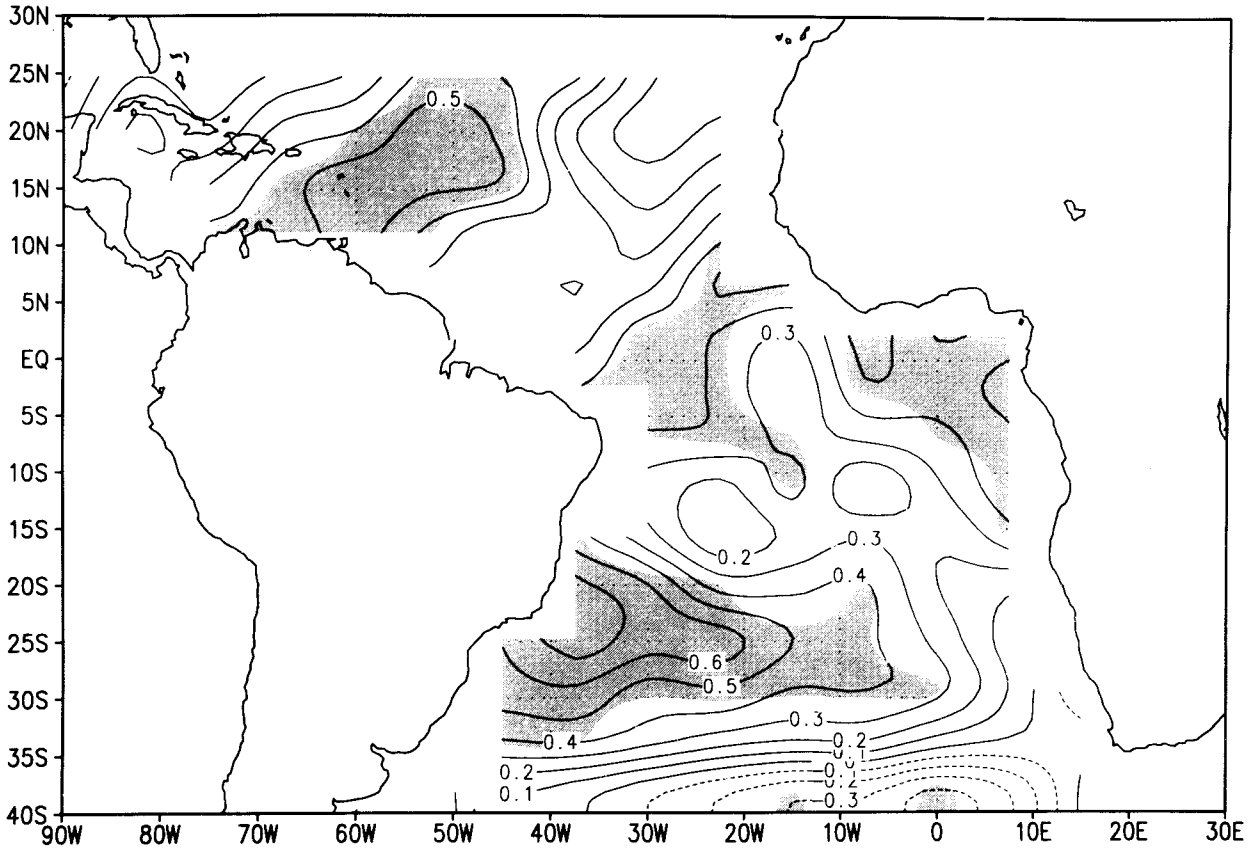
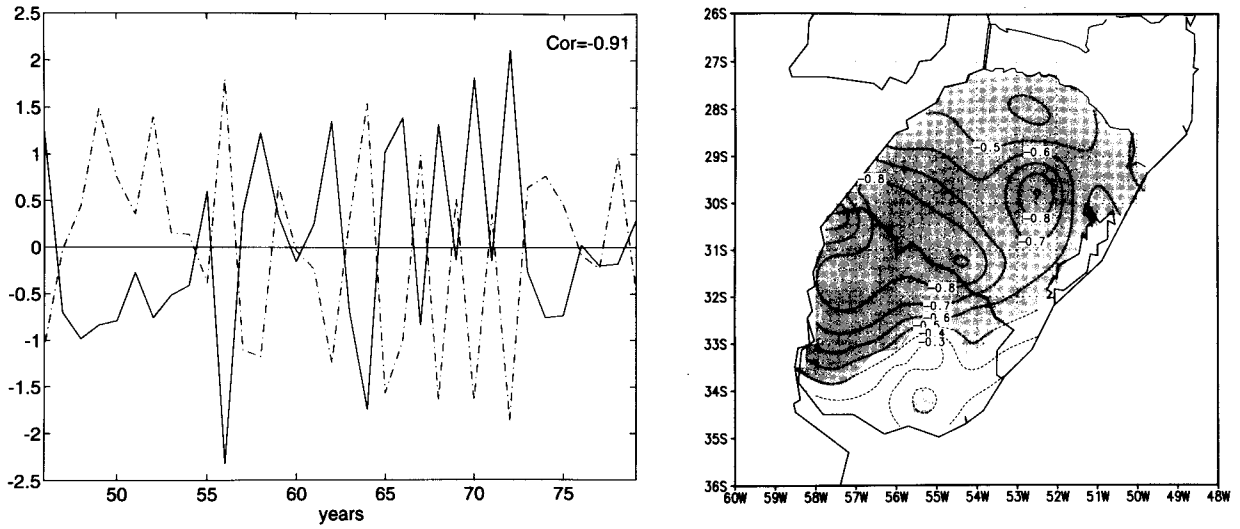


FIG. 7. As in Fig. 6 except for the SST anomalies in the Atlantic Ocean.

→

FIG. 8. First canonical vectors and canonical patterns for Nov–Feb and SST anomalies in both Pacific and Atlantic oceans: (upper left) canonical vectors  $u_1$  (solid) and  $v_1$  (dashed), (upper right) canonical pattern  $h_1$ , (middle and bottom) portions of the canonical pattern  $g_1$  corresponding to the Pacific and Atlantic Ocean, respectively. Shaded areas represent regions with values that are significant at the 95% level.

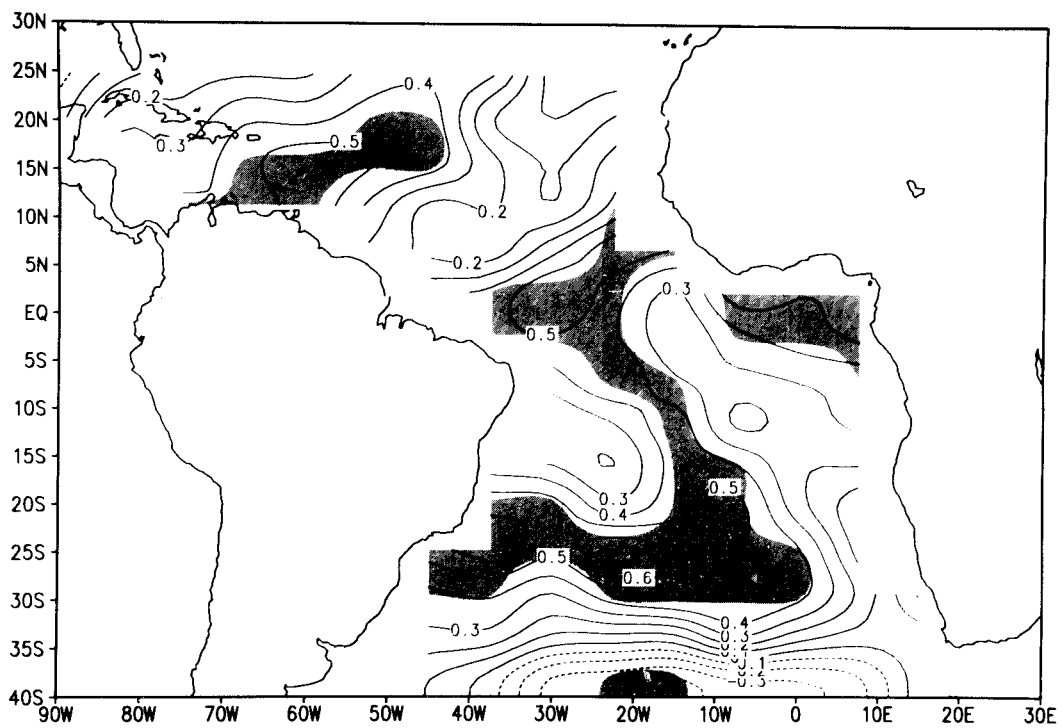
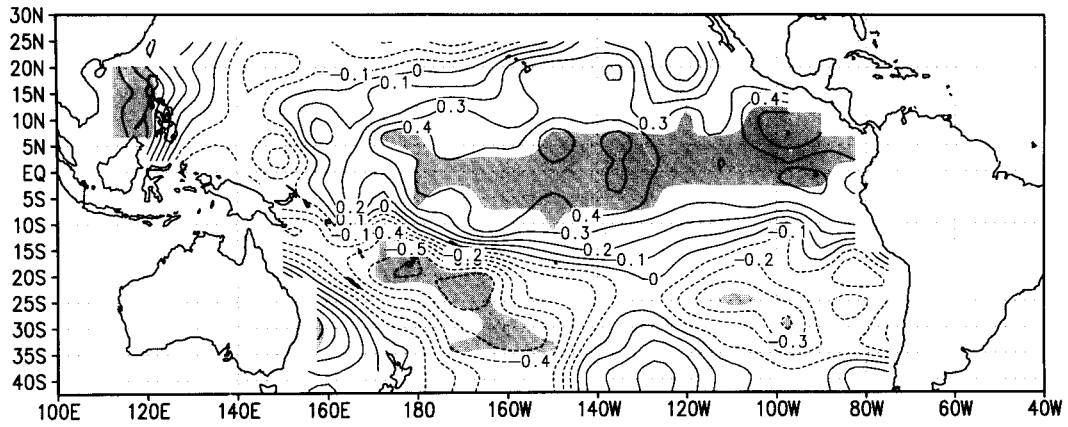
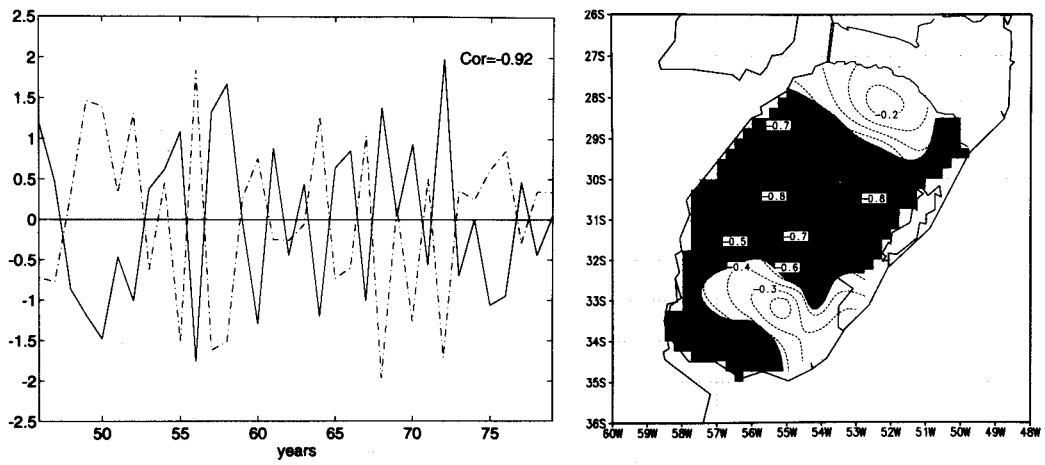


TABLE 3. November–February: Relationships between SST anomalies in the Pacific (upper row), Atlantic (middle row), and Pacific–Atlantic (bottom row) and rainfall anomalies in URSOL (see Figs. 6, 7, and 8) (w, warm; c, cold): CEEP, central and eastern equatorial Pacific; SWTP, southwestern tropical Pacific; SWSA, southwestern subtropical Atlantic; EEQA, eastern equatorial Atlantic; NWTa, northwestern tropical Atlantic; WEQA, western equatorial Atlantic. The third column shows the years in which  $\mu_1$  reaches the first three maxima (first row) and minima (second row). The fourth column shows the absolute value of the first canonical correlation coefficient.

SST anomaly	Sector and type of rainfall anomaly		Year	$ \mu_1 $
CEEP w, SWTP c CEEP c, SWTP w	Central	Wet–Dry	1972, 1957, 1965 1949, 1952, 1956	0.86
SWSA w, EEQA w, WEQA w, NWTa w SWSA c, EEQA c, WEQA c, NWTa c	Northern and central	Wet–Dry	1972, 1970, 1966 1956, 1964, 1948	0.91
CEEP w, SWTP c, SWSA w, EEQA w, WEQA w, NWTa w CEEP c, SWTP w, SWSA c, EEQA c, WEQA c, NWTa c	Central	Wet–Dry	1972, 1958, 1968 1956, 1950, 1960	0.92

some differences between corresponding values in Figs. 6–8. For example, when one considers the two oceans together instead of separately, the sector with negative and significant values is somewhat more developed in the SPCZ region and more sharply defined in the tropical Atlantic. Figure 8 also shows that  $h_1$  has negative values in the entire URSOL. The sector with significant values is very similar to that obtained with the SST anomalies in the Pacific only. It appears, therefore, that SST anomalies in the Pacific and Atlantic oceans tend to reinforce one another in terms of their impacts on rainfall in URSOL.

#### d. Discussion

Table 3 presents a summary of the results obtained in this case. For the period November–February, the most significant values of rainfall anomalies are in the middle western subregion of URSOL for all configurations of SST anomalies. A particular example of agreement between our analyses and their observational counterpart was 1972 (see Table 3), which had a strong El Niño event characterized by positive rainfall anomalies during November–February. Consistently, the three configurations of SST anomalies indicate “wet–warm” relationships. On the other hand, 1976 was also a year with positive rainfall anomalies during this period, and no configuration of SST anomalies indicates “wet” relationships.

The links found between SST anomalies in the Pacific and rainfall anomalies in URSOL appear to be integral components of relationships between ENSO and rainfall in southeastern South America. The positive and significant correlations between SST anomalies in the eastern equatorial Pacific and rainfall in southeastern South America during the period November–February are consistent with the findings of Ropelewski and Halpert (1987, 1989) and Pisciotto et al. (1994). Our results also show that SST anomalies in the southwestern tropical Pacific are linked to rainfall anomalies in URSOL.

This link is, at least in part, another component of ENSO. Lau and Chan (1983), for example, showed that ENSO is associated with an eastward displacement of the SPCZ, which is consistent with the SST anomalies we are considering.

The links between SST anomalies in the southwestern Atlantic and rainfall anomalies in URSOL can also be another manifestation of remote ENSO impacts. The studies of Grimm and Silva Dias (1995) suggest that remote effects of an eastward displacement of convection in the SPCZ can result in the enhancement of a trough in southeastern South America. Casarin and Kousky (1986) demonstrated that an anomalous trough in southeast Brazil is associated with an enhancement of convection in the SACZ, which is consistent with episodes of rainfall anomalies in the region. The SST anomalies in the southwestern subtropical Atlantic can actually be the manifestation of complex perturbations in the atmospheric and oceanic circulations associated with ENSO. The precise mechanisms for connection between atmospheric and oceanic anomalies in the tropical Pacific and Atlantic are not yet fully understood. The oceanic region east of URSOL can be influenced by the variability in the convergence between the warm Brazil current flowing southward along the Brazilian coast and the cold Malvinas current flowing northward along the coast of southern South America. The precise location of this convergence and of the boundary between warmer waters to the north and colder waters to the south might have complex feedbacks with the southeast extension of the SACZ.

The significance of the relationships between SST anomalies in the northwestern tropical Atlantic and rainfall anomalies in URSOL is also consistent with links found by Enfield (1996) between the SST anomalies in the Pacific and Atlantic. The relationships between SST anomalies in the equatorial Atlantic and rainfall anomalies in southeastern South America (SSA) are less robust. This is also consistent with the weak interannual

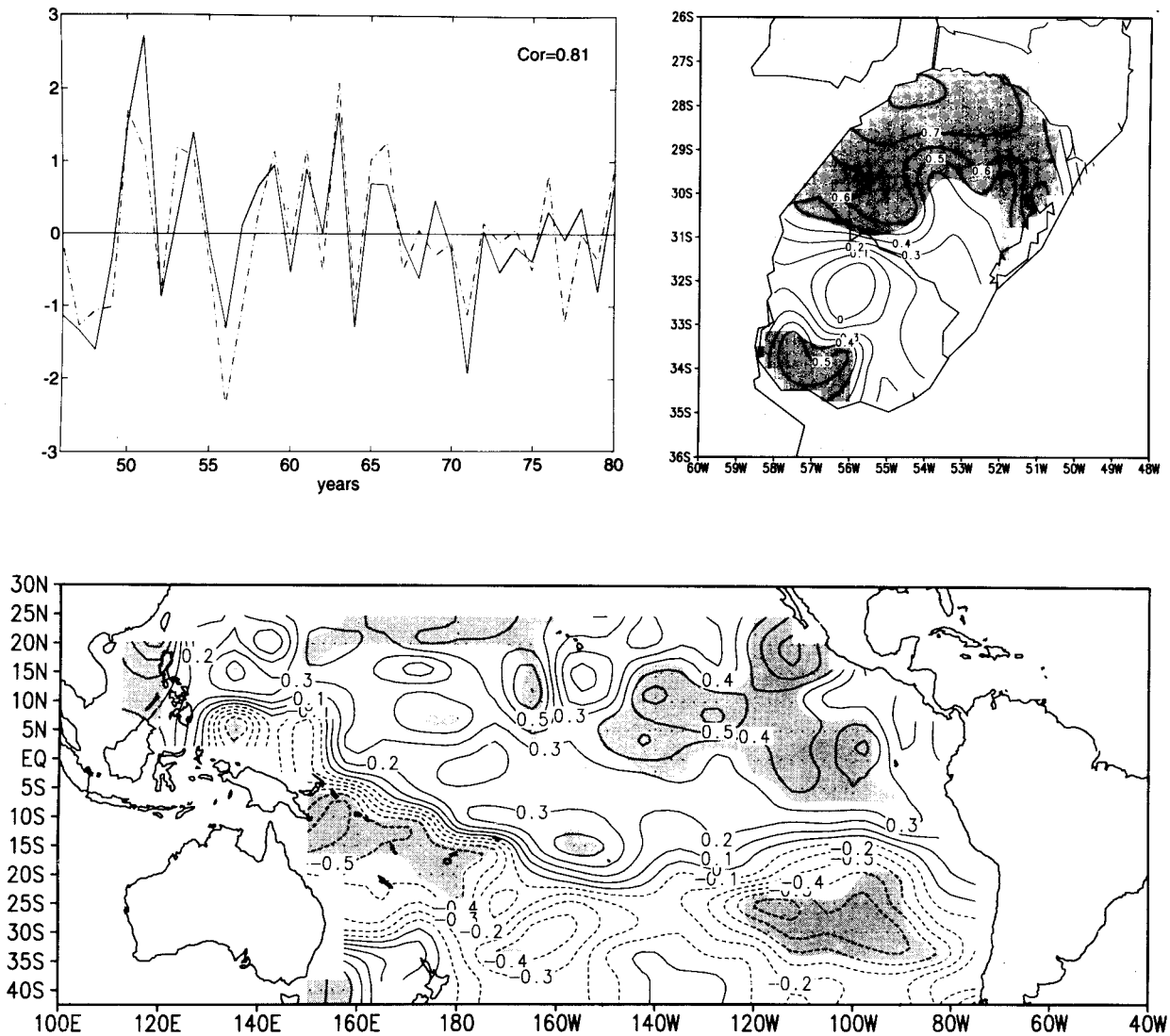


FIG. 9. As in Fig. 6 except for Oct–Dec.

variability in the tropical Atlantic suggested by the studies of Zebiak (1993).

A meaningful question raised by these results is whether SST anomalies in the Atlantic contribute on their own to rainfall anomalies in URSOL. The answer to this question seems to be on the affirmative, since the absolute value of the correlation between  $u_1$  and  $v_1$  (i.e.,  $\mu_1$ ) increases from 0.86 (Pacific SST only) to 0.91 and 0.92 (Atlantic SST only and Pacific–Atlantic SST, respectively). This is not unexpected since SST anomalies in the southwestern subtropical Atlantic might influence rainfall along the coastal region, where local effects can reinforce and even sporadically overcome remote effects. Another meaningful issue is whether SST anomalies in the Atlantic, independent of ENSO, contribute to rainfall anomalies in URSOL. Again, the answer to this question seems to be the affirmative, since

the years when both  $u_1$  and  $v_1$  peak (see Table 3) do not necessarily coincide when we consider the two oceans either separately or jointly.

### 6. Relationships between anomalies in rainfall and SST: October–December

#### a. SST anomalies in the Pacific Ocean

In this case (see Fig. 9), the correlation between  $u_1$  and  $v_1$  is 0.81, which implies that the patterns of SST and rainfall anomalies associated with the first canonical modes tend to have the same correspondence in sign as  $g_1$  and  $h_1$ . Figure 9 shows that  $g_1$  has positive values to the north and negative values to the south of a northwestern–southeastern line across the Pacific Ocean. There is a major sector with significant positive values

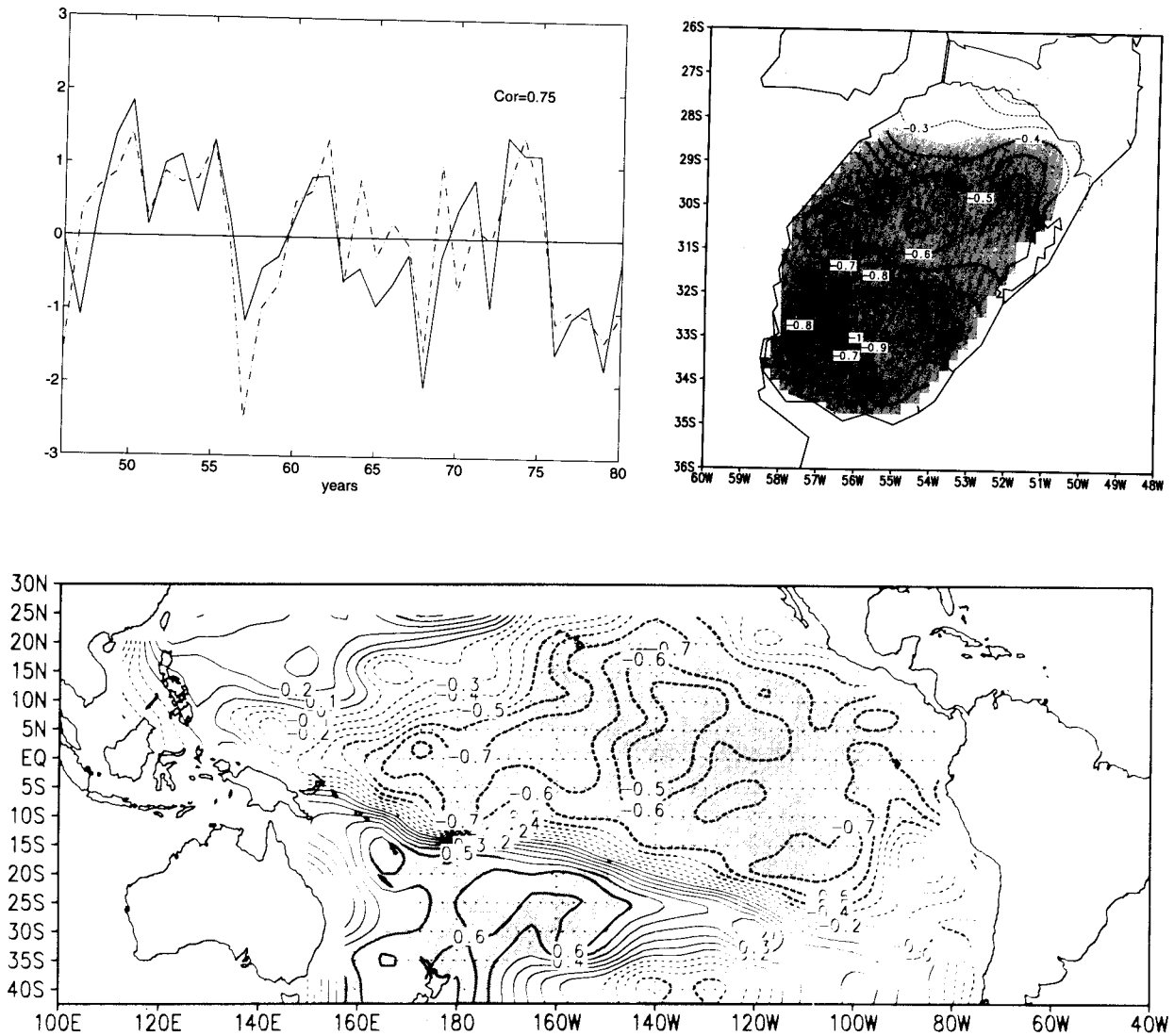


FIG. 10. Second canonical vectors and canonical patterns for Oct–Dec and SST anomalies in the Pacific Ocean: (upper left) canonical vectors  $u_2$  (solid) and  $v_2$  (dashed), (upper right) canonical pattern  $h_2$ , and (bottom) canonical pattern  $g_2$ . Shaded areas represent regions significant at the 95% level.

in the northeastern tropical Pacific (NETP), and two major sectors with significant negative values in the southeastern tropical Pacific (SETP) (under the subtropical high) and the SWTP. Figure 9 also shows that  $h_1$  has positive values over practically the entire URSOL. There are two sectors with significant values in the northern and southwestern URSOL. These results support the existence of wet (dry) rainfall anomalies in the northern and southwestern sectors of URSOL simultaneous with warm (cold) SST anomalies in the NETP and cold (warm) SST anomalies in the SETP sector and SPCZ region.

The correlation between  $u_2$  and  $v_2$  is also high in this case (0.75). Figure 10 shows that  $g_2$  has mostly negative values except for the southwestern Pacific. Most negative values in the tropical and northeastern Pacific and

most positive values in the southwestern subtropical Pacific are significant. A band of large gradients of  $g_2$  extends from the SPCZ in a southeast direction to the coast of South America. Figure 10 shows that  $h_2$  has negative values in the entire URSOL. Except for the northernmost sector, all of these values are significant. These results support the existence of dry (wet) rainfall anomalies in almost the entire URSOL simultaneous with cold (warm) SST anomalies in the tropical and northern eastern Pacific east of about  $160^\circ\text{E}$  and warm (cold) SST anomalies in the SPCZ region.

#### b. SST anomalies in the Atlantic Ocean

In this case (see Fig. 11), the correlation between  $u_1$  and  $v_1$  is  $-0.82$ , which implies that the patterns of SST

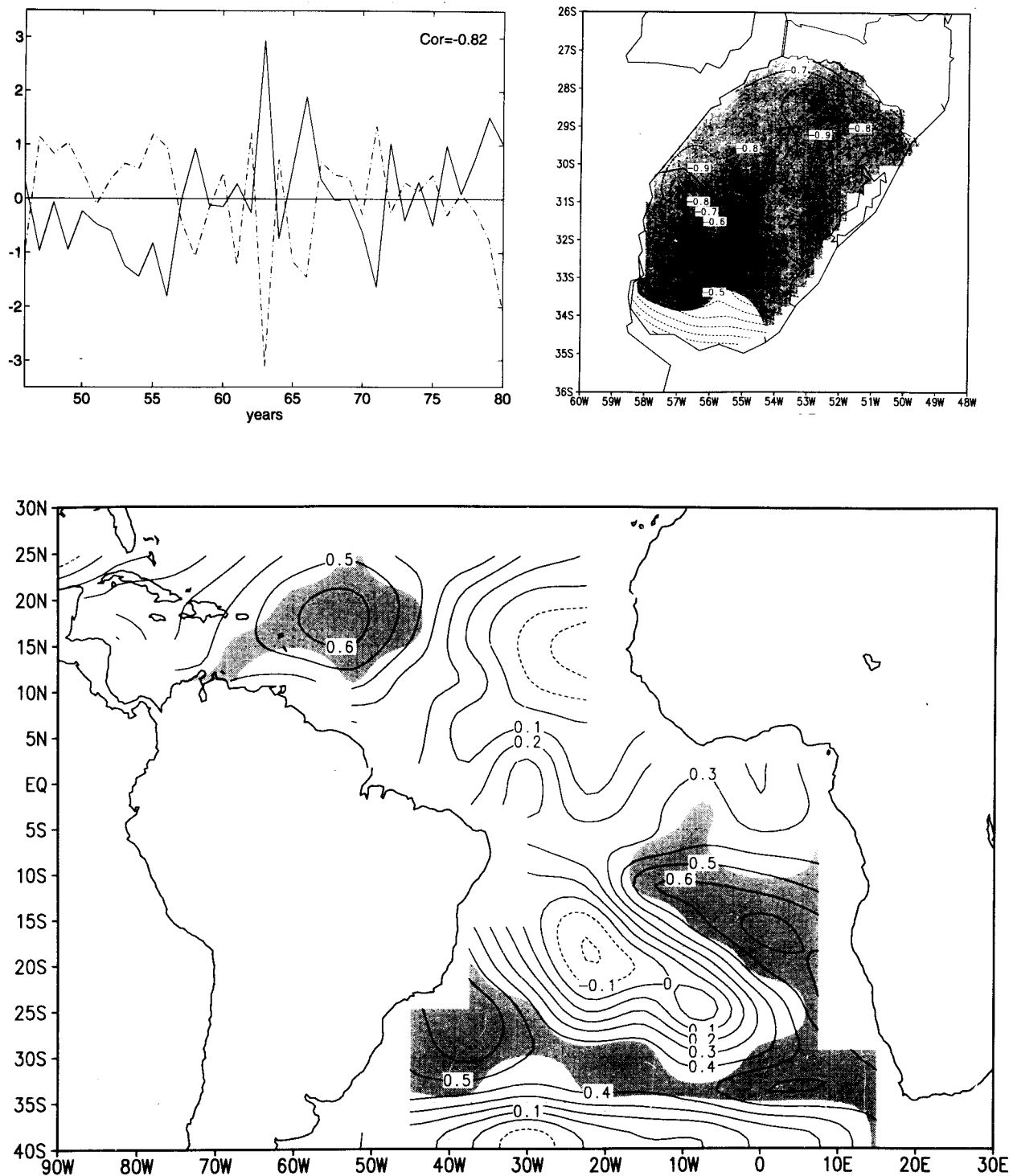


FIG. 11. As in Fig. 6 except for Oct–Dec and the Atlantic Ocean.

and rainfall anomalies associated with the first canonical modes tend to have the *opposite* correspondence in sign as  $g_1$  and  $h_1$ . Figure 11 shows that  $g_1$  has mostly positive values. There are significant values in the southwestern subtropical, southeastern equatorial, and northwestern

tropical sectors. In general, the sectors with significant values are fairly similar to the SWSA, EEQA, and NWTa obtained for the period November–February with the SST anomalies in the Atlantic Ocean (see Fig. 7). Figure 11 also shows that  $h_1$  has negative and sig-

nificant values over URSOL, except along the southern boundary of the region. These results support the existence of relationships between rainfall and SST anomalies similar to those found for the period November–February.

### c. SST anomalies in the Pacific and Atlantic oceans

In this case (see Fig. 12) the correlation between  $u_1$  and  $v_1$  is 0.86, whose magnitude is larger than those obtained for the individual ocean basins. Figure 12 shows that in the Pacific Ocean  $g_1$  has negative values north of about 15°S and predominantly positive values south of that latitude. There are significant negative values of  $g_1$  in the equatorial and northern Pacific (EQNP), and significant positive values in the SPCZ and other regions of minor extension. In the Atlantic,  $g_1$  presents negative values almost everywhere. Negative significant values of  $g_1$  appear in the SWSA and the NWTA. These results are in fair agreement with those obtained for October–December by using the SST anomalies in each ocean separately (see Figs. 9 and 11). Figure 12 also shows that  $h_1$  has negative values over the entire region, with significant values in Rio Grande do Sul and southwestern Uruguay. These results are consistent with wet (dry) rainfall anomalies in Rio Grande do Sul and southwestern Uruguay and simultaneous cold (warm) SST anomalies in the SPCZ region, and warm (cold) SST anomalies in the equatorial and northern Pacific, as well as in the SWSA and NWTA.

### d. Discussion

Table 4 presents a summary of the results obtained in this case. As expected, these results are similar to those obtained for the period November–February. There is, however, one interesting difference between the results for the two periods: the years with peaks in the magnitude of  $v_1$  obtained by using the SST anomalies in the Pacific and Atlantic do not necessarily coincide with those obtained for either  $v_1$  or  $v_2$  by using SST anomalies in the Pacific only. SST anomalies in the Atlantic, therefore, may contribute on their own to rainfall anomalies in URSOL.

## 7. Relationships between anomalies in rainfall and SST: April–July

### a. SST anomalies in the Pacific Ocean

In this case (see Fig. 13), the correlation between  $u_1$  and  $v_1$  is  $-0.81$ , which implies that the patterns of SST and rainfall anomalies associated with the first canonical modes tend to have the opposite correspondence in sign as  $g_1$  and  $h_1$ . The pattern of  $g_1$  is generally similar to that obtained for the period October–December by using the SST anomalies in the Pacific Ocean but with opposite signs (see Fig. 9). Figure 13 also shows that  $h_1$

has positive values in the southern sector of URSOL and negative values in the northern sector. The only sector with significant values of  $h_1$  is the northern half of Rio Grande do Sul. A comparison between these results and those shown in Figs. 6 and 9 suggests that the impact of SST anomalies in the Pacific on rainfall anomalies in URSOL moves north from November–February to April–July.

These results support the existence of dry (wet) rainfall anomalies in the northern sector of URSOL simultaneous with warm (cold) SST anomalies in the southeastern tropical Pacific (SETP) and northern central Pacific (NOCP), and cold (warm) SST anomalies in the southeastern extratropical Pacific (SECP). We can speculate that cold SST anomalies in the southeastern extratropical Pacific are consistent with the development of a blocking high near the west coast of South America and that such a development prevents frontal systems from reaching URSOL.

### b. SST anomalies in the Atlantic Ocean

In this case (see Fig. 14), the correlation between  $u_1$  and  $v_1$  is  $-0.80$ , which implies that the patterns of SST and rainfall anomalies associated with the first canonical modes tend to have the *opposite* correspondence in sign as  $g_1$  and  $h_1$ . Figure 14 shows that  $g_1$  has a pattern of alternate signs as the latitude varies. The only sector with positive and significant values is in the SWSA eastward from URSOL. Figure 14 also shows that  $h_1$  has negative values in almost the entire URSOL, of which all except for those corresponding to the southernmost sector are significant. These results support the existence of relationships between wet (dry) rainfall anomalies in the southern sector of URSOL and warm (cold) SST anomalies in the SACZ region.

### c. SST anomalies in the Pacific and Atlantic oceans

In this case (see Fig. 15), the correlation between  $u_1$  and  $v_1$  is  $-0.79$ , whose absolute value is slightly smaller than those obtained for the individual ocean basins. Figure 15 shows that  $g_1$  has negative values in almost the entire tropical Pacific and positive values south of 25°S. There is a sector with negative and significant values extending approximately around the Niño3 region from the northern subtropics to the western equatorial to the southern tropical Pacific (NSST), which differs substantially from that obtained with the SST anomalies in the Pacific only (see Fig. 13). There are also smaller sectors with positive and significant values of  $g_1$  south of 35°S. In the Atlantic,  $g_1$  has negative values in the Southern Hemisphere except along the African coast in the subtropics. There are sectors with small geographical extent and significant negative values in the southern subtropical and northwestern tropical Atlantic. Figure 15 also shows that  $h_1$  has positive values over all of

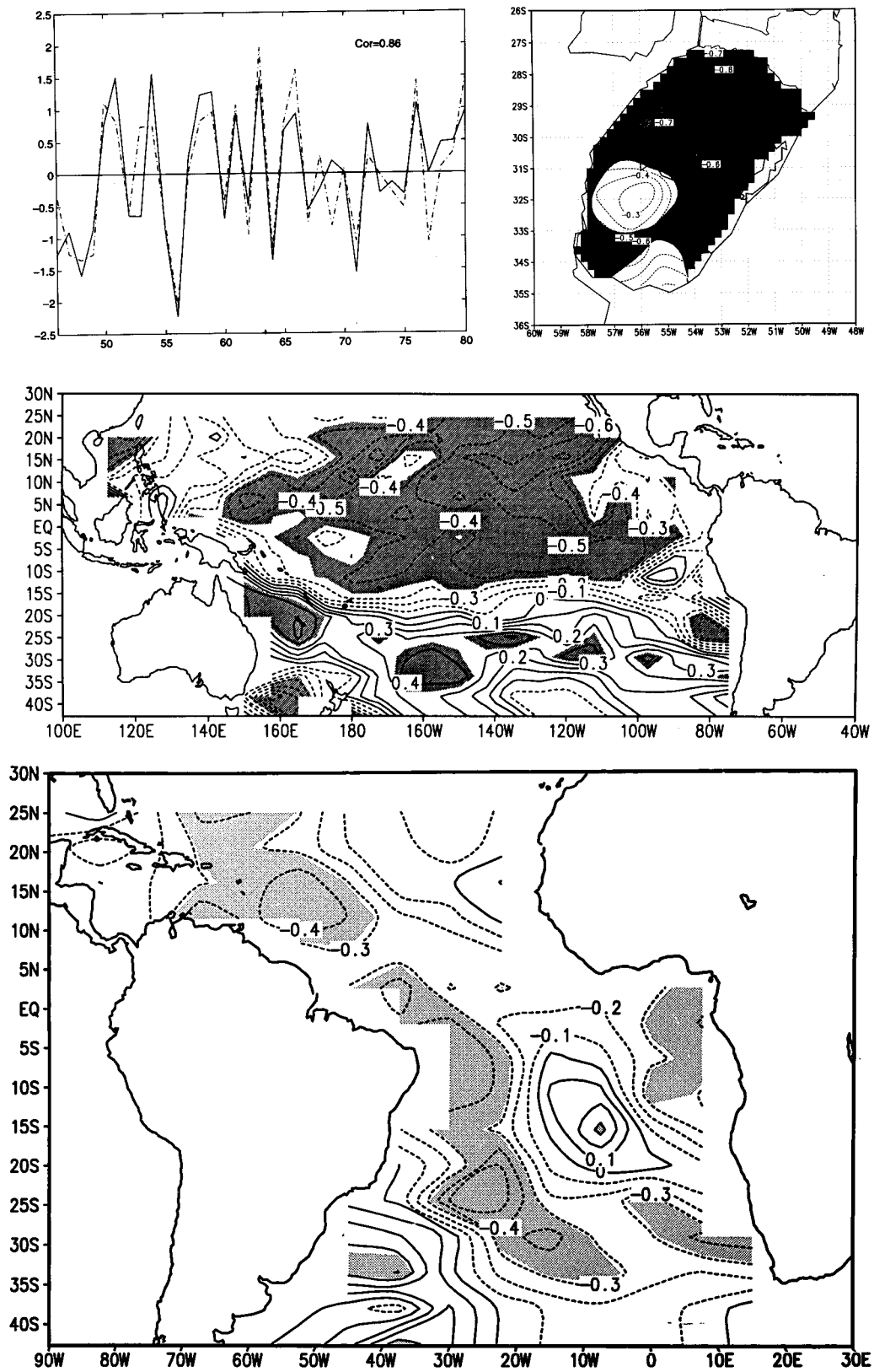


FIG. 12. As in Fig. 8 except for Oct–Dec.

TABLE 4. October–December: Relationships between SST anomalies in the Pacific (upper row), Atlantic (middle row), and Pacific–Atlantic (bottom row) and rainfall anomalies in URSOL (see Figs. 9, 11, and 12) (w, warm; c, cold): NETP, northeastern tropical Pacific; SETP, southeastern tropical Pacific; SWTP, southwestern tropical Pacific; SWSA, southwestern subtropical Atlantic; EEQA, eastern equatorial Atlantic; NWTa, northwestern tropical Atlantic; EQNP, equatorial and northern Pacific; SPCZ, south Pacific convergence zone; MTA, middle tropical Atlantic. The third column shows the years in which  $\mu_1$  reaches the first three maxima (first row) and minima (second row). The fourth column shows the absolute value of the first canonical correlation coefficient.

SST anomaly	Sector and type of rainfall anomaly		Year	$ \mu_1 $
NETP w, SETP c, SWTP c NETP c, SETP w, SWTP w	Northern	Wet–Dry	1951, 1963, 1954	0.81
			1971, 1948, 1947	
SWSA w, EEQA w, NWTa w SWSA c, EEQA c, NWTa c	Northern and central	Wet–Dry	1963, 1966, 1979	0.82
			1956, 1971, 1954	
SPCZ c, EQNP w, MTA w NWTa w, SWSA w SPCZ w, EQNP c, MTA c NWTa c, SWSA c	Northern and central	Wet–Dry	1954, 1951, 1963	0.86
			1956, 1948, 1971	

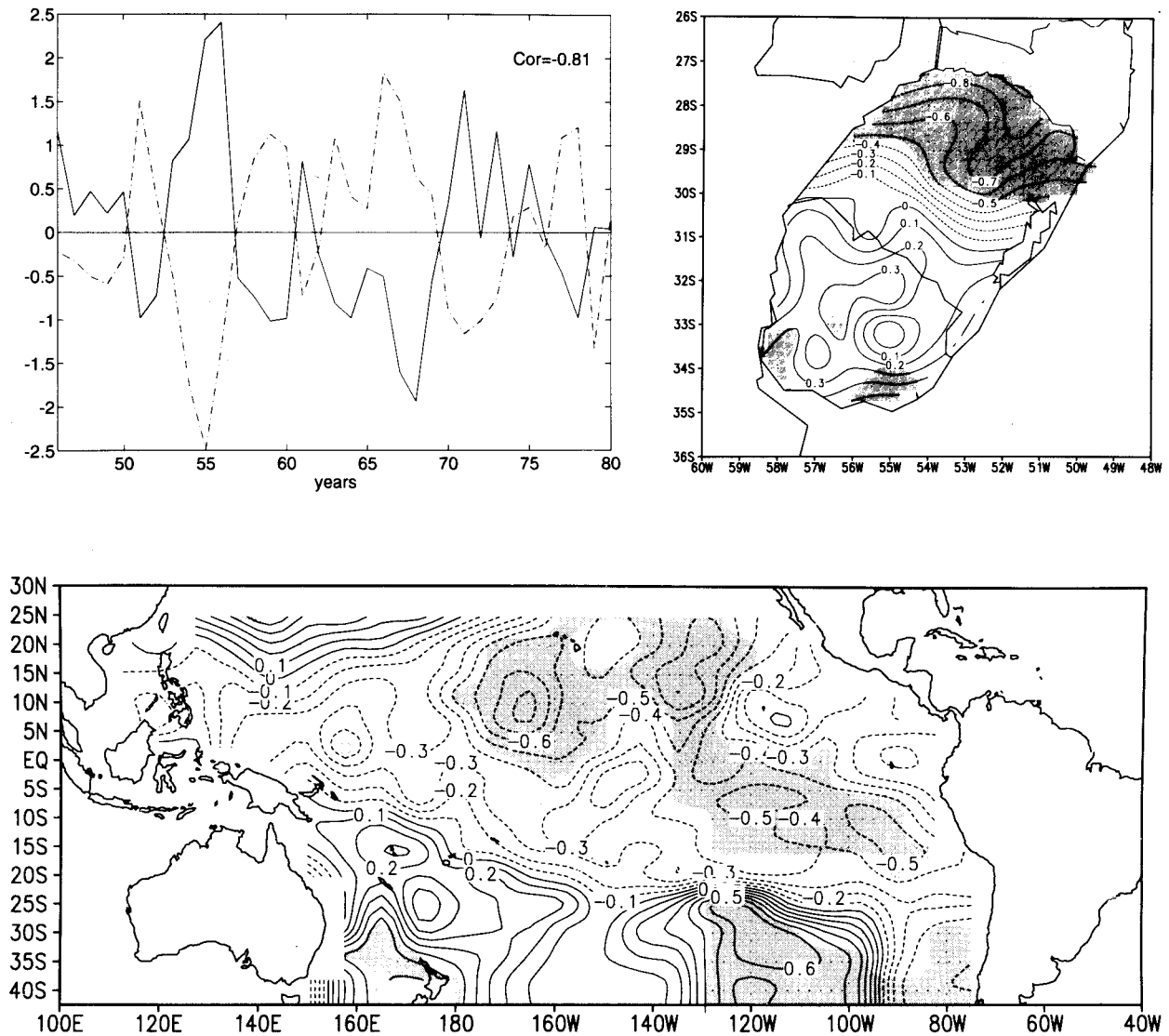


FIG. 13. As in Fig. 6 except for Apr–Jul.

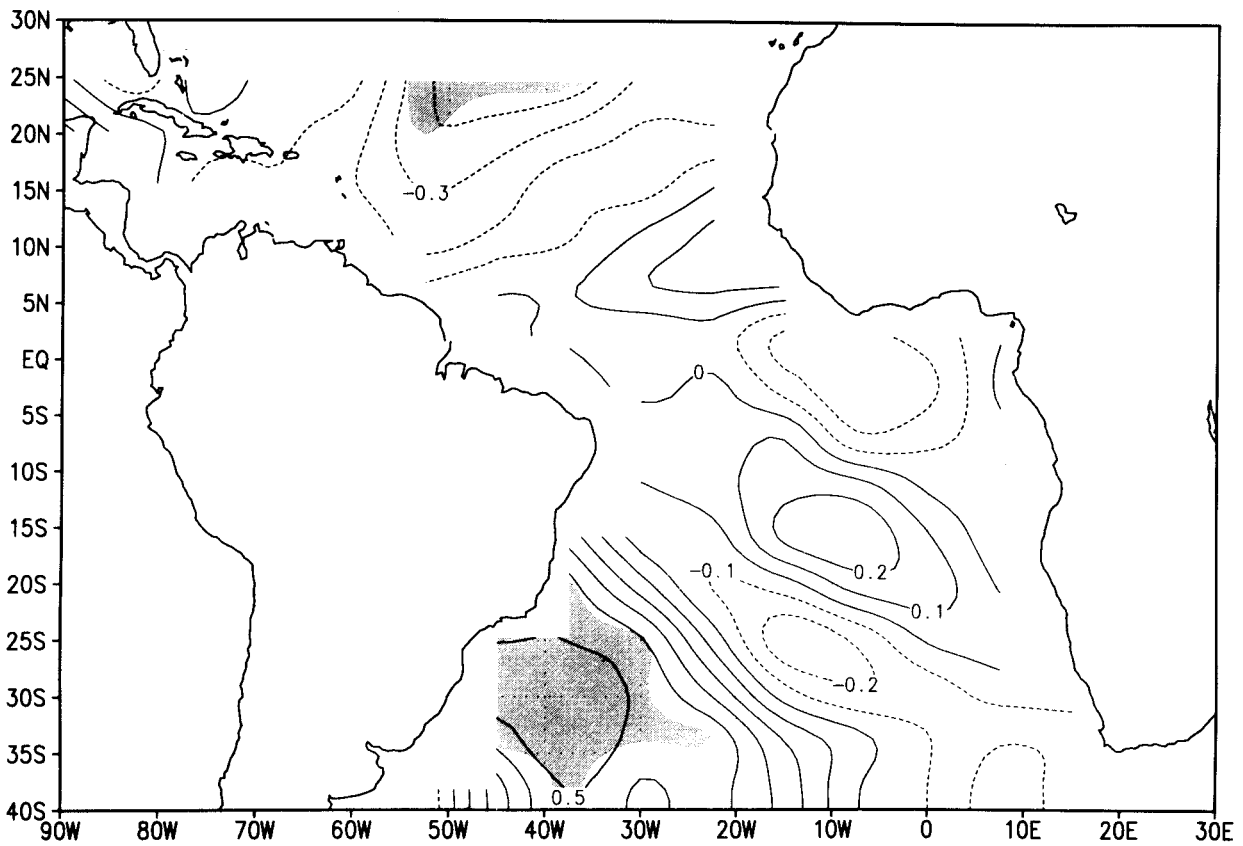
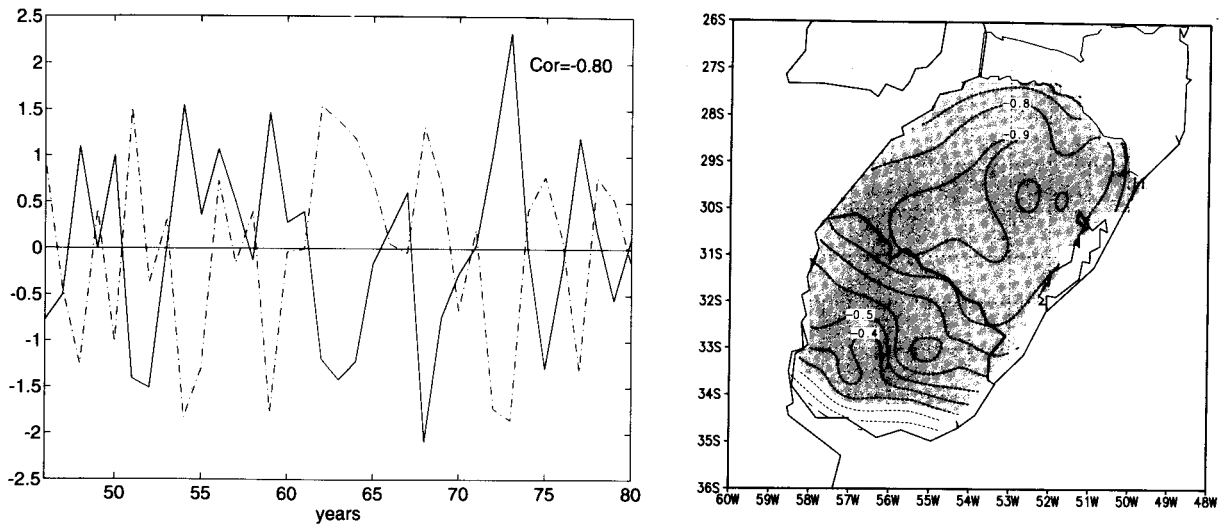


FIG. 14. As in Fig. 6 except for Apr–Jul and the Atlantic Ocean.

URSOL. There is a sector with significant values in northern Uruguay and southern Rio Grande do Sul, and another with smaller extent in southwestern Uruguay. These results support the existence of wet (dry) rainfall anomalies in northern and southwestern Uruguay and

warm (cold) SST anomalies in the NSST. For this period, therefore, the relationships between the simultaneous fields of SST anomalies and rainfall anomalies in URSOL seem to weaken when both oceans are considered together for analysis.

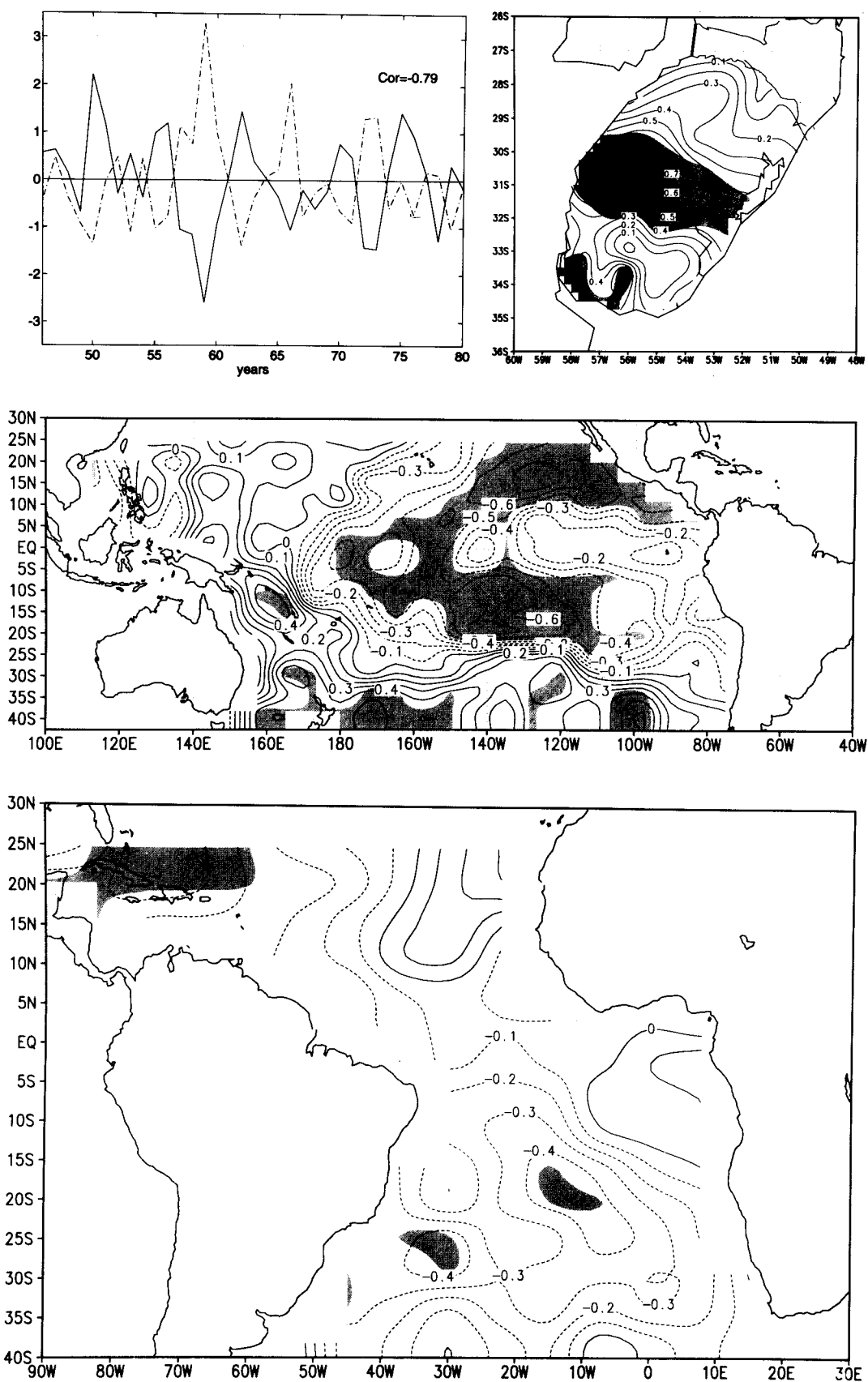


FIG. 15. As in Fig. 8 except for Apr-Jul.

TABLE 5. April–July: Relationships between SST anomalies in the Pacific (upper row), Atlantic (middle row), and Pacific–Atlantic (bottom row) and rainfall anomalies in URSOL (see Figs. 13, 14, and 15) (w, warm; c, cold): SETP, southeastern tropical Pacific; NOCP, northern central Pacific; SECP, southeastern extratropical Pacific; SWSA, southwestern subtropical Atlantic; NSST, northern subtropics to the western equatorial to the southern tropical Pacific. The third column shows the years in which  $\mu_1$  reaches the first three maxima (first row) and minima (second row). The fourth column shows the absolute value of the first canonical correlation coefficient.

SST anomaly	Rainfall anomaly in URSOL		Year	$ \mu_1 $
SETP c, NOCP c, SECP w SETP w, NOCP w, SECP c	Northern	Wet–Dry	1956, 1955, 1971 1968, 1967, 1959	0.81
SWSA w SWSA c	Entire region	Wet–Dry	1973, 1954, 1959 1968, 1953, 1963	0.80
NSST w NSST c	Central	Wet–Dry	1959, 1973, 1972 1950, 1975, 1962	0.92

#### d. Discussion

Table 5 presents a summary of the results obtained in this case. The sharp contrast between the patterns of  $g_1$  shown in Figs. 13 and 15 suggests that when SST anomalies are considered simultaneously in both oceans, the links between rainfall anomalies in URSOL and SST anomalies are weaker than when the oceans are considered separately. Table 2 shows that the fraction of variance explained by the first canonical vector for Atlantic SST is, by far, the largest. This result suggests that SST anomalies in the southwestern Atlantic Ocean have a more direct influence on rainfall anomalies in URSOL than the SST anomalies in the Pacific Ocean during April–July. Such an influence is at work whether the oceanic pattern shown in Fig. 14 is a consequence of remote forcings or generated from phenomena local to the Atlantic Ocean.

## 8. Two case studies of anomalous rainfall

### a. The southern spring of 1970

In October–January 1970, precipitation was fairly high in Uruguay (Pisciottano et al. 1994, see their Figs. 7a and 8a). Since 1970 was a high SO index year, below median rainfall could be expected during October–December in Uruguay. Inspection of the first canonical mode for the case of SST anomalies in the Atlantic Ocean does not provide any guidance on this issue. On the other hand,  $u_1$  has its second maximum for 1970 in the case of SST anomalies in the Atlantic Ocean during November–February (see Table 3), which is consistent with a warm–wet relationship. Again, the influence of Atlantic SST anomalies appears to be a key factor for the development of this event of anomalously high rainfall.

### b. The southern fall of 1959

In April 1959, precipitation was extremely heavy in almost all of Uruguay and southern Rio Grande do Sul. One rainfall station recorded 943 mm, and the average over several stations in the region was around 500 mm. Since neither 1958 nor 1959 were El Niño years, this

extreme event of positive rainfall anomalies cannot be thought of in the context of the influence of ENSO on local rainfall. Table 5 shows that when we consider the SST anomalies in the Pacific Ocean during April–July, 1959 has the third minimum of  $u_1$ , which is consistent with a “dry–warm” relationship between the SETP, NOCP, and the northernmost region of URSOL and a “dry–cold” relationship between the SECP and the same region in URSOL. Nevertheless, if we consider the SST anomalies in the Atlantic Ocean, 1959 has the third maximum of  $u_1$ , which is consistent with a wet–warm relationship between the entire URSOL and a sector of the Atlantic situated eastward from it (see Fig. 14). When we consider SST anomalies in both the Pacific and Atlantic oceans during April–July, we find that 1959 has the absolute minimum of  $u_1$ , which is consistent with a wet–warm relationship between the rainfall anomalies in the central sector of URSOL and SST anomalies in the eastern Pacific off the equator and the northwestern tropical Atlantic (see Fig. 15). Our results suggest, therefore, that the episode of anomalously high rainfall in URSOL during the southern fall of 1959 was linked to SST anomalies in the Atlantic Ocean.

## 9. Conclusions

We have analyzed the mean precipitation and its anomalies in a region of southeastern South America that extends roughly east of 58.5°W, from 35° to 27°S. This region comprises Uruguay and the Brazilian state of Rio Grande do Sul. Our analyses were based on data from 40 stations almost evenly distributed in the region.

We find that the distribution of total rainfall in the region is fairly even throughout the year. On average, the largest rainfall falls in September–October with a secondary maximum in March–April, and the minimum falls in November–December. Local rainfall, on the other hand, has important spatial and temporal variability. A principal component analysis of monthly rainfall reported by stations shows that the largest variability appears as a west–east (inland–coastal) dipole with largest positive departures from the annual mean in the west during early fall and midspring, and in the east along the Atlantic coast during winter. The second mode of

rainfall variability appears as a south–north dipole with the largest positive departures from the annual mean in the south during late summer and late fall, and in the north during early spring and early summer. The third mode appears primarily as a north–south dipole along the western boundary of the region, with the largest positive departures from the annual mean in southwestern Uruguay during fall, and in northwestern Rio Grande do Sul during early spring. These modes explain 60%, 19%, and 8% of the total variance. Five subregions could be identified according to the local characteristics of their annual rainfall cycle.

Our results confirm that rainfall anomalies in the region are linked with ENSO during November–February and, to a lesser extent, during October–December. For these two periods, it is apparent that rainfall anomalies are also associated with SST anomalies in the SPCZ and the SACZ regions. In October–December, there are also links with the subtropical high region in the southeastern Pacific. For April–July, the links with ENSO are at best indirect.

For November–February, the patterns of  $g_1$  and  $h_1$  based on the SST anomalies in either the Pacific, Atlantic, or Pacific and Atlantic oceans are remarkably similar to each other. One can speculate as to whether the SST anomalies in both oceans are primarily independent of each other or if, in this period, the anomalies in one of the oceans (presumably the Pacific) primarily drive those in the other ocean. For the three periods considered in this study, we found that some relationships between SST anomalies in the Pacific Ocean and rainfall anomalies in URSOL are in general agreement with others reported by previous studies for selected years, while other regions show an opposite behavior. This result should be used with caution, since CCA is a linear technique. Taking into account the proximity of the Atlantic Ocean to URSOL, it is not yet clear whether some (or all) of the patterns of SST anomalies in the Atlantic Ocean shown in this paper are the signature of either global or regional features (or both). This concern is of particular relevance to the pattern of significant SST anomalies found for the period April–July because the strongest relationship between rainfall anomalies in URSOL and SST anomalies for this period were found for the Atlantic Ocean.

In all periods considered in this study, we found that rainfall variability in Uruguay and the Brazilian state of Rio Grande do Sul is linked to SST anomalies in both the Pacific and Atlantic oceans. This apparent association between an atmospheric phenomenon and oceanic phenomena in two oceans suggests several possible scenarios. First, *both* rainfall anomalies in the region *and* SST anomalies in the southwestern subtropical Atlantic can be the manifestation of complex perturbations in the atmospheric and oceanic circulations associated with ENSO but are relatively independent of each other. This seems to be the case for the periods November–February and October–December, when ENSO is in its mature

phase. Second, events in the Pacific can produce a lagged response in the Atlantic, which may become a dominant contributor to rainfall anomalies in the region selected for this study. This will depend on the strength of teleconnections between the atmospheric circulation in southeastern South America and the adjacent ocean and the equatorial Pacific, which can vary during the seasonal cycle. In this scenario, the impact of SST anomalies in the Atlantic may be stronger, although the existence of this oceanic feature ultimately depends on the Pacific. Third, there can be SST anomalies in the Atlantic that are independent of ENSO and that contribute on their own to rainfall anomalies in URSOL. One of the last two scenarios seems to apply in the period April–July, when the Atlantic signal is stronger.

The underlying issue is the extent to which the two oceans evolve independently, especially during the extremes of the Southern Oscillation. In these periods, our results provide a strong motivation for further research on the precise mechanisms for connection between oceanic anomalies in the Pacific and Atlantic, as well as for production of operational SST forecasts of the coupled atmosphere–ocean system in the Atlantic Ocean.

*Acknowledgments.* A large part of this research was performed when the first two authors participated in the First Training Course on Practical and Theoretical Aspects of Short-Term Climate Prediction sponsored by the International Research Institute for Climate Prediction (IRI-NOAA) held at Lamont-Doherty Earth Observatory (LDEO). Special thanks are due to IRI and LDEO for their support, G. Berri for his encouragement during the course of this study, and N. Graham and Y. Kushnir for sharing their expertise on statistical techniques applied to atmospheric sciences. G. Pisciotano, S. Hastenrath, and an anonymous reviewer provided useful comments on earlier versions of this work. The authors also wish to thank DINAMET, IPAGRO, and INEMET for providing the rainfall data, and LDEO for the SST data. Additional support was provided by Consejo de Investigaciones Científicas y Técnicas (CONICYT, Uruguay), through Project 117/94, and NOAA and NSF under Grants NA56GPO222 and ATM9122153.

#### REFERENCES

- Aceituno, P., 1988: On the functioning of the Southern Oscillation in the South American sector. Part I: Surface climate. *Mon. Wea. Rev.*, **116**, 505–524.
- Barnett, T. P., and R. W. Preisendorfer, 1987: Origins and levels of monthly and seasonal forecast skill for United States surface air temperatures determined by canonical correlation analysis. *Mon. Wea. Rev.*, **115**, 1825–1850.
- Casarin, D. P., and V. E. Kousky, 1986: Precipitation anomalies in the southern part of Brazil and variations of the atmospheric circulation. *Rev. Bras. Meteor.*, **1**, 83–90.
- Enfield, D. B., 1996: Relationships of inter-American rainfall to tropical Atlantic and Pacific SST variability. *Geophys. Res. Lett.*, **23**, 3305–3308.

- Gan, M. A., and V. B. Rao, 1991: Surface cyclogenesis over South America. *Mon. Wea. Rev.*, **119**, 1293–1302.
- Graham, N. E., J. Michaelsen, and T. P. Barnett, 1987a: Investigations of the El Niño Southern Oscillation with statistical models. 1: Predictor field characteristics. *J. Geophys. Res.*, **92**, 14 251–14 270.
- , —, and —, 1987b: Investigations of the El Niño Southern Oscillation with statistical models. 2: Model results. *J. Geophys. Res.*, **92**, 14 271–14 290.
- Grimm, A. M., and P. L. Silva Dias, 1995: Analysis of tropical–extratropical interactions with influence functions of a barotropic model. *J. Atmos. Sci.*, **52**, 3538–3555.
- Lau, K. M., and P. J. Sheu, 1988: Annual cycle, quasi-biennial oscillation, and Southern Oscillation in global precipitation. *J. Geophys. Res.*, **93**, 10 975–10 988.
- Lau, N., and P. H. Chan, 1983: Short-term climate variability and atmospheric response to observed outgoing longwave radiation. Part I: Simultaneous relationship. *J. Atmos. Sci.*, **40**, 2735–2750.
- , and M. J. Nath, 1990: A general circulation model study of the atmospheric response to extratropical sea surface temperature anomalies observed in 1950–1979. *J. Climate*, **3**, 965–989.
- Logue, J. J., 1984: Regional variations in the annual cycle of rainfall in Ireland as revealed by principal component analysis. *J. Climatol.*, **4**, 597–607.
- Mechoso, C. R., and G. Pérez, 1992: Streamflow in southeastern South America and the Southern Oscillation. *J. Climate*, **5**, 1535–1539.
- North, G. R., T. L. Bell, R. F. Cahalan, and F. J. Moeng, 1982: Sampling errors in the estimation of empirical orthogonal functions. *Mon. Wea. Rev.*, **110**, 699–706.
- Pisciottano, G. J., A. F. Díaz, G. Cazes, and C. R. Mechoso, 1994: El Niño–Southern Oscillation impact on rainfall in Uruguay. *J. Climate*, **7**, 1286–1302.
- Preisendorfer, R. W., 1988: *Principal Component Analysis in Meteorology and Oceanography*. Elsevier, 418 pp.
- Prohaska, F., 1976: The climate of Argentina, Paraguay and Uruguay. *Climates of Central and South America*, W. Schwerdtfeger, Ed., World Survey of Climatology, Vol. 12, Elsevier, 13–112.
- Rao, V. B., and K. Hada, 1990: Characteristics of rainfall over Brazil: Annual variations and connections with the Southern Oscillation. *Theor. Appl. Climatol.*, **42**, 81–91.
- Ropelewski, C. F., and M. S. Halpert, 1987: Global and regional scale precipitation patterns associated with the El Niño/Southern Oscillation. *Mon. Wea. Rev.*, **115**, 1606–1626.
- , and —, 1989: Precipitation patterns associated with high index phase of Southern Oscillation. *J. Climate*, **2**, 268–284.
- Silva Dias, M. A., 1987: Sistemas de mesoescala e previsao de tempo a curto prazo. *Rev. Bras. Meteor.*, **2**, 133–150.
- Terra, R., and G. J. Pisciottano, 1994: Regionalización del Uruguay según el ciclo anual de precipitaciones mediante “Cluster Analysis.” *Memorias XVI Congreso Latinoamericano de Hidráulica*, Santiago, Chile, IAHR, 227–236.
- Velasco, I., and J. M. Fritsch, 1987: Mesoscale convective complexes over the Americas. *J. Geophys. Res.*, **92**, 9591–9613.
- Zebiak, S. E., 1993: Air–sea interaction in the equatorial Atlantic region. *J. Climate*, **6**, 1567–1586.